

Research on the blockage effect in a shock tube

Dong Shao

Ocean College, Zhejiang University, Zhoushan, 316021, China.

22134079@zju.edu.cn

Abstract. The shock tube is a crucial experimental apparatus in the field of explosive impact. Limited research has been conducted on the visualization of the internal flow field in shock tubes under blockage conditions, and there is a lack of comprehensive understanding of the mechanisms behind blockage effects. This paper presents experimental and numerical investigations into the propagation of shock waves inside a shock tube and their interaction with obstructive elements. Blockage effect experiments were conducted on a shock tube test platform, where pressure data were obtained through a pressure monitoring system. Additionally, schlieren imaging technology was employed to visualize the evolution of shock wave fronts. A two-dimensional numerical model of the shock tube was established using Fluent software, and the computed results exhibited excellent agreement with the experimental data, confirming the accuracy of the numerical model. The mechanism of the blockage effect was revealed through analysis of pressure-time curves and images depicting the evolution of shock wave fronts. Furthermore, adjustments to parameters on the validated numerical model allowed for analysis and comparison of different blockage ratios. The results indicate that the disturbance to the flow field caused by the blockage effect is primarily due to the reflection of shock waves between the front surface of the obstructive element and the shock tube wall. This reflection leads to differences in pressure curves compared to free-field conditions, and such differences increase with higher blockage ratios.

Keywords: Shock Tube, Shock Wave, Blockage Effect, Visualization.

1. Introduction

Large-scale explosion-driven shock tubes serve as ideal experimental platforms in the field of explosion effects, offering a cost-effective and low-risk alternative to live explosive experiments. Typically, these tubes are cylindrical and sealed at both ends, with a diaphragm dividing them into a high-pressure driver section and a low-pressure driven section. Shock waves are generated through the rupture of the diaphragm. With a history spanning over a century, shock tubes have seen continuous refinement in their working principles, control techniques, and parameter design methods in the last three decades [1]. The fundamental purpose of shock tubes is to simulate shock waves in a free-field explosive environment and apply the resulting shock load to objects. However, during experiments, the propagation of shock waves in the shock tube flow field is influenced by the obstruction of objects and the constraints of the tube walls. This results in a deviation between the actual evolution of wave fronts and that in a free-field condition, leading to the phenomenon known as the blockage effect [2].

Several scholars have previously investigated the evolution of flow fields within shock tubes. Jiang et al. [3] achieved flow field visualization through a lens-type shock tube cross-section, obtaining high-

precision flow field images and observing the formation processes of spherical waves, vortices, and Mach waves. Murugan et al. [4] studied the changes in the flow field behind the shock wave at the shock tube outlet, predicting the formation and evolution of vortices through numerical methods. Validation was completed through experimental schlieren images and smoke flow visualization. Arun et al. [5] tested the interaction of shock waves within shock tubes with obstacles of different geometric shapes, studying the phenomena of shock wave reflection and diffraction in complex channels. They also compared the effects of different geometric designs on shock wave attenuation. The blockage ratio is typically defined as the ratio of the obstructing surface area to the cross-sectional area of the shock tube, and when the blockage ratio is high, experimental data may become less accurate. Some scholars have researched blockage effects and related numerical algorithms. Zhao et al. [6], using LS-Dyna software, established a three-dimensional physical model of a tunnel, characterizing explosion waveforms, maximum explosion overpressure, and the arrival time of peak pressure near obstacles with different blockage ratios. Li [7] focused on the interaction between explosion waves and obstacles using commercial CFD software, comparing and analyzing the differences in shock wave reflection and diffraction under obstacles of different geometric sizes. Yao et al. [8] quantitatively studied numerical results of shock tubes under different blockage ratios, revealing significant influences on pressure data on the surface of test objects when the blockage ratio is high. However, there has been limited research on the visualization of flow fields within shock tubes under blockage conditions, and there is a significant gap in understanding the mechanism behind blockage effects.

This paper comprehensively investigates the interaction between shock waves and obstructive elements within shock tubes through experiments and numerical simulations. In contrast to previous research, the novelty of this paper lies in the validation of numerical model reliability through monitored data obtained from experiments and visualized flow field images. Additionally, parameters were adjusted on the validated model to study the differences in results under various blockage ratios.

2. Experimental Procedure

The shock tube experimental platform is illustrated in Figure 1(a), and its schematic diagram is shown in Figure 1(b). The apparatus is divided into a driver section and a driven section by a diaphragm. Within the driven section, there are observation windows, and an obstruction is fixed within the range of the window using an L-shaped steel tube. The obstruction is designed as a 2mm thick circular thin plate, with its front surface area accounting for 20% of the cross-sectional area of the shock tube. Its axis aligns with the axis of the shock tube. The upper end of the L-shaped steel tube is connected to the shock tube wall, and a pressure sensor can be externally connected to the surface of the obstruction through the steel tube to monitor pressure at the center of the front surface of the obstruction. Pressure sensor interfaces are arranged at regular intervals on the upper wall surface, and, during the experiment, the wall surface located 0.1m from the front surface of the obstruction is selected for pressure monitoring. Additionally, schlieren imaging systems are positioned on both sides of the window to capture images of the flow field evolution.

The experimental procedure is as follows: Firstly, the installation of the shock tube and obstruction, as shown in Figure 1(b), is completed. Subsequently, the experimental monitoring system is set up. Pressure sensors are installed at the center of the front surface of the obstruction and the shock tube wall, and the sensor, signal amplifier, and oscilloscope are connected correctly. Light sources and high-speed cameras are arranged on either side of the window and adjusted to ensure that the captured images cover the window area as extensively as possible, presenting a clear view of the flow field in front of the obstruction [9]. After completing the aforementioned preparations, the experimental operation commences. A small amount of gas is injected into the high-pressure section from a gas cylinder to check for leaks in the shock tube system. Once leakage is confirmed to be absent, the formal inflation process begins. High-pressure gas is slowly introduced into the driver section until the pressure gauge reading reaches 5MPa, causing the diaphragm to rupture and generating a shock wave rapidly moving into the driven section, thus loading the obstruction. Finally, experimental data processing is carried out

based on parameters of sensors, high-speed cameras, and other equipment to obtain pressure-time curves and schlieren images.

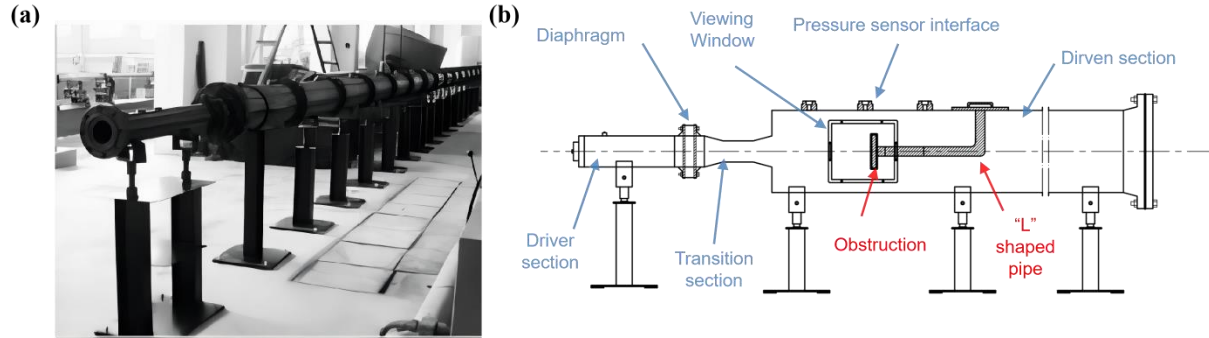


Figure 1. Shock tube platform: (a) actual device and (b) schematic diagram.

3. Numerical Model

The numerical model was constructed using the CFD software FLUENT. Considering the high-speed movement characteristics of shock waves, a density-based solver was selected to solve the governing equations, and the standard k-epsilon model was applied to simulate turbulence. The Roe-FDS scheme was chosen to compute the flux at flow discontinuities. The fluid density within the flow field was determined using the ideal gas law.

The computational domain and boundary conditions for the two-dimensional shock tube model are depicted in Figure 2. The domain was divided into the high-pressure driver section on the left side of the diaphragm and the low-pressure driven section on the right side. During the initialization phase, the initial pressure of the high-pressure section was set to the experimental driver pressure of 5MPa. An outflow boundary condition was applied at the exit, and all other external boundaries were treated as no-slip walls. In accordance with the experimental conditions, the length L of the driven section was set to 10m, the diameter D was set to 234mm, and the diameter d of the obstruction was determined such that $d = \sqrt{0.2D}$ to ensure a blockage ratio matching the experimentally set 20%. The obstruction was positioned along the shock tube axis, with two pressure monitoring points set on its front surface center and 0.1m upstream from the front surface. To simplify the calculations, the model omitted the supports behind the obstruction since they have minimal impact on the flow field in front of the obstruction.

The grid generation method is illustrated in Figure 3. The grid region near the obstruction was locally refined, with the size of the innermost layer closest to the object surface set to 0.01mm to accurately capture complex physical phenomena such as shock wave reflection and diffraction. Boundary layer grids were established near the shock tube wall, with the size of the first layer in the wall boundary layer set to 0.05mm. The overall grid growth rate across the entire computational domain was maintained below 1.2. Following grid independence verification, the grids in non-refined regions were ultimately set to $1\text{mm} \times 1\text{mm}$, controlling the computational duration while ensuring accuracy.

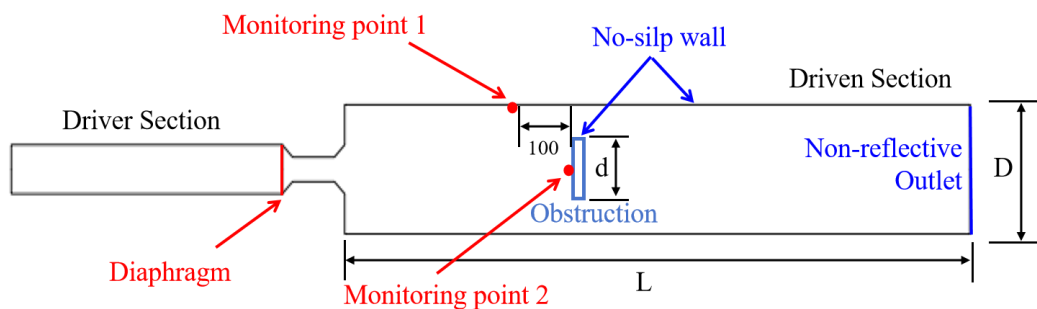


Figure 2. Computational model of the shock tube.

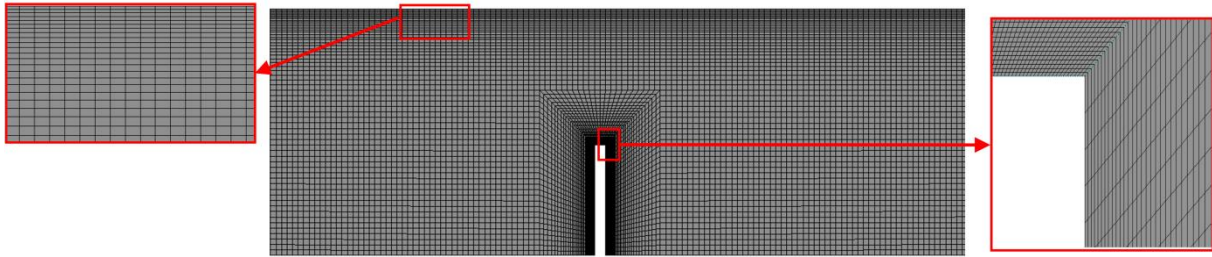


Figure 3. Grid scheme for the FLUENT model.

4. Results and Discussion

Figure 4 presents a comparison between the pressure-time curves obtained in the experiment and the numerical simulation results. There is a high degree of agreement between the experimental and numerical results, with a close match in overall trends and individual peaks. This demonstrates the high accuracy of the numerical model. For ease of subsequent description, the time at which the incident shock wave reaches the front surface of the obstruction is defined as the zero moment. Therefore, the incident wave arrives at monitoring point 1 before the zero moment, as indicated by the first rising edge in the curve in Figure 4(a). The first peak in this curve corresponds to the peak overpressure of the incident wave, reaching approximately 100kPa, consistent with the experimental expectation. As shown in Figure 4(b), the pressure curve at monitoring point 2 reaches its peak at the zero moment, with the peak of the reflected wave being about 2.5 times that of the incident wave. The features on the curve are related to the reflected wave and blockage effect, which will be detailed in conjunction with the evolution of the wave fronts.

Figure 5 displays schlieren images obtained in the experiment, depicting the evolution of wave fronts before and after the shock wave reaches the object surface. Figure 6 shows pressure distribution maps at different times obtained through numerical simulation. Due to pressure discontinuities on both sides of the shock wave fronts, the pressure distribution maps effectively represent the position and propagation characteristics of the wave fronts. The evolution characteristics of the wave fronts in these two sets of images exhibit strong consistency, further indicating the reliability of the numerical model in predicting the flow field inside the shock tube. Since the range captured by the schlieren system is insufficient to completely cover the entire flow field within the window, adjustments were made during the experiment to align the circular field of view precisely with the obstruction and be tangent to the lower surface of the shock tube. This arrangement allowed the schlieren images to capture as much information as possible about the reflected waves between the obstruction and the tube wall. In comparison to experimental images, pressure distribution maps obtained through numerical simulation provide more comprehensive information about the flow field and allow a rough assessment of the shock wave intensity based on the color of the wave fronts. Considering that the diffraction waves behind the obstruction have a minor impact on the flow field, the following discussion primarily focuses on the propagation and reflection phenomena of shock waves in front of the obstruction.

The initially incident wave propagates from left to right, reaching the surface of the obstruction and undergoing reflection, forming reflected waves that propagate upstream. This process creates a high-pressure region near the front surface of the obstruction, with a maximum overpressure of approximately 242kPa, matching the first peak at monitoring point 2 in Figure 4(b). As the rarefaction waves from the upper and lower edges of the obstruction propagate towards the high-pressure region, the wave fronts of the reflected waves gradually become curved. Around 0.2ms, the reflected waves reach the shock tube wall, reflecting on the wall to form wall-reflected waves. The wall-reflected waves on both sides gradually propagate towards the center of the flow field, subsequently acting on the surface of the obstruction and reaching monitoring point 2 at around 0.4ms, corresponding to the second peak in Figure 4(b). Additionally, as shown in Figure 6(f), the reflected waves are about to reach the position of monitoring point 1 shortly after 0.4ms, explaining the arrival of the second peak at monitoring point 1

in Figure 4(a) around 0.5ms. Subsequently, the wall-reflected waves on both sides meet on the axis and propagate to the other side, reflecting on the wall again, thus repeating the process and continually perturbing the flow field. Consequently, pressure curves at both monitoring points undergo multiple oscillations in the subsequent period. However, the amplitude of pressure curve oscillations gradually decreases, attributed to the attenuation of reflected wave intensity in the subsequent propagation, as clearly observed in the changing colors near the reflected wave fronts in the pressure cloud map in Figure 6. This process reveals the disturbance mechanism of the blockage effect on the flow field in the shock tube, describing the mechanism influencing the experimental data.

To mitigate the impact of the blockage effect on experimental data, it is advisable to reduce the blockage ratio of the shock tube experiment, making the pressure load on the object surface closer to that of free-field conditions. Investigating this issue through repeated experiments with varying parameters would consume significant time and cost. Numerical methods can more efficiently yield results. While keeping the obstruction diameter d constant in the numerical model, the diameter of the driven section of the shock tube D was progressively increased to reduce the blockage ratio. Calculations were conducted at blockage ratios of 20%, 15%, 10%, 5%, and 1%, and the differences in the pressure load processes at the midpoint of the front surface of the obstruction were compared, as shown in Figure 7. As the blockage ratio decreases, the second peak in the curve diminishes and arrives later, indicating that the action of the wall-reflected waves on the surface of the obstruction occurs later and with less intensity. Particularly, when the blockage ratio drops to 5%, low-intensity disturbances can only be identified in the curve around 1ms, while at this time, the curve under high blockage ratio has already begun the second oscillation. Furthermore, as the blockage ratio drops to 1%, there is no discernible impact of reflected waves on the pressure curve at monitoring points within 4ms, making the curve equivalent to that of free-field conditions. The analysis results above demonstrate that the increasing amplitude and frequency of pressure curve oscillations can reflect the strengthening of the disturbance to the flow field caused by the blockage effect. Therefore, under specific shock tube experimental conditions, one can assess the similarity between the curve under blockage conditions and the curve under free-field conditions in advance to analyze the degree of the blockage effect, thereby guiding shock tube experiments.

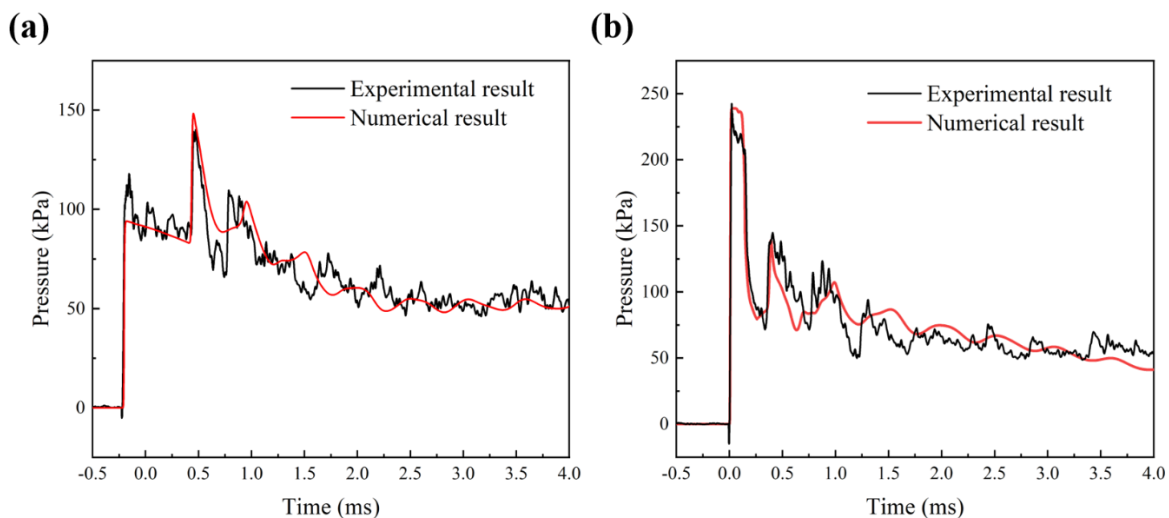


Figure 4. Comparison of experimental and numerical pressure-time curves at each monitoring point: (a) monitoring point 1 and (b) monitoring point 2.

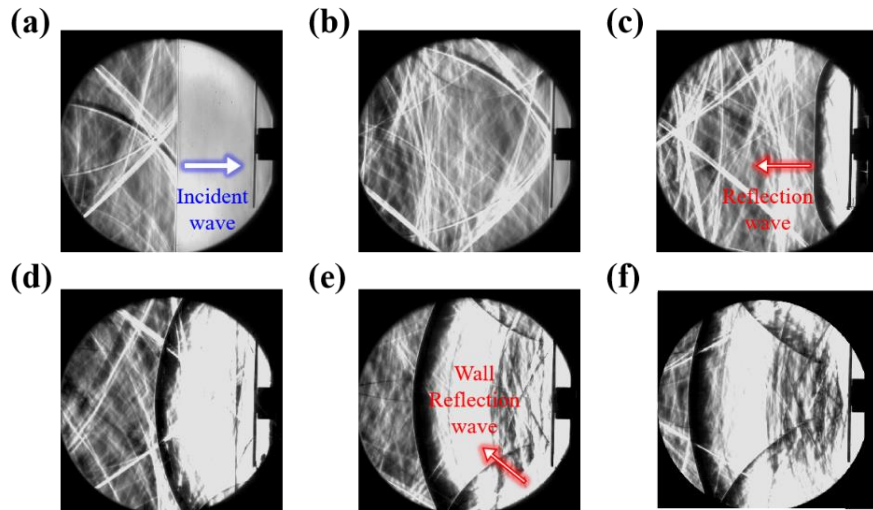


Figure 5. Schlieren images at different moment: (a) -0.1ms, (b) 0ms, (c) 0.1ms, (d) 0.2ms, (e) 0.3ms and (f) 0.4ms.

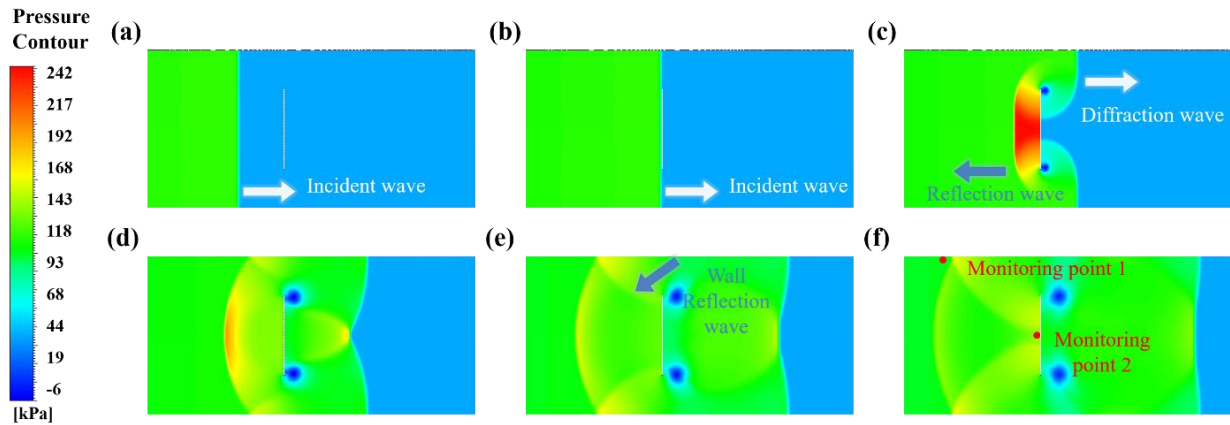


Figure 6. Pressure contours obtained from the numerical model at: (a) -0.1ms, (b) 0ms, (c) 0.1ms, (d) 0.2ms, (e) 0.3ms and (f) 0.4ms.

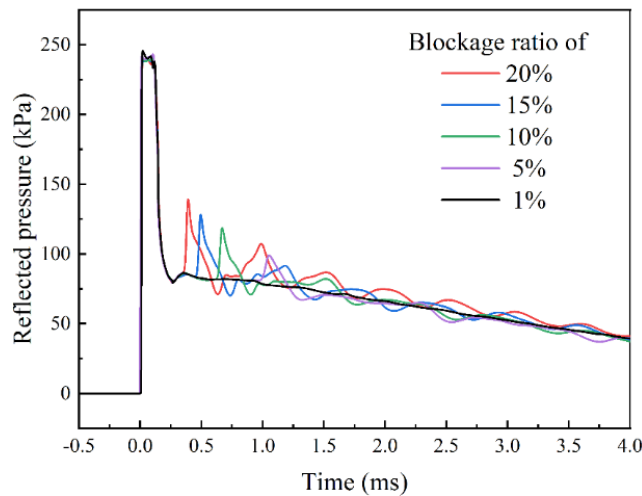


Figure 7. Comparison of reflected pressure histories at different blockage ratio

5. Conclusion and Outlook

This paper provides a comprehensive exposition and analysis of the blockage effect phenomenon in a shock tube apparatus, combining experimental and numerical methods. The use of a schlieren imaging system in the experiment facilitated the visualization of the flow field, capturing critical information. A corresponding numerical model was established based on the CFD software FLUENT, and the highly consistent results between the numerical and experimental outcomes attest to the reliability of numerical calculations. Through a comprehensive analysis of these results, the paper elucidates the propagation and reflection processes of shock waves. By integrating the peak features on the pressure curves, the mechanism of the blockage effect is revealed. Building upon this foundation, the numerical model was employed to investigate the differences in pressure curves under various blockage ratios. Notably, the pressure curve at a blockage ratio of 1% closely resembled the characteristics of the free-field curve. As the blockage ratio increased, the similarity between the curve and the free-field curve gradually diminished, indicating a strengthening degree of the blockage effect.

This study specifically analyzes the blockage effect of a 2mm-thick wall panel under shock tube experimental conditions with a driving pressure of 5MPa and an incident wave peak overpressure of approximately 100kPa. In the next step, the influence of other parameters on the blockage effect in the shock tube, such as incident wave intensity and obstruction thickness, will be analyzed. Additionally, future research could propose a computational method to quantitatively assess the degree of blockage effect, enabling a quantitative evaluation of the differences in data obtained under specific experimental conditions and free-field conditions.

References

- [1] Balan G S and Raj S A 2023 *Int. J. Impact Eng.* 172 104406
- [2] Saathoff P J and Melbourne W H 1987 *J. Wind. Eng. Ind. Aerod.* 26 353-70.
- [3] Jiang Z, Takayama K, Babinsky H and Meguro T 1997 *Shock Waves* 7 151-62
- [4] Murugan T, De S, Dora C L, Das D and Kumar P 2013 *Fluid Dyn. Res.* 45 025506
- [5] Arun K R and Pathak V 2021 *Def. Technol.* 17 1840-51
- [6] Zhao X, Chen C, Shi C, Chen J, Chen Q and Zhao D 2021 *J. Therm. Anal. Calorim.* 143 3245-56
- [7] Li J and Hao H 2021 *Process Saf. Environ. Prot.* 145 94-109.
- [8] Yao Z, Ren H, Shen Z and Wang Z 2012 *Prot. Eng.* 34 18-23.
- [9] Bunjong D, Pussadee N and Wattanakasiwich P 2018 *J. Phy.: Conf. Ser.* 1144 012097